Contents

3. Models of the Variability of Atmospheric Properties

C.H. Humphrey
Visidyne, Inc.
Burlington, Mass.

C.R. Philbrick
Air Force Geophysical Laboratory
Hanscom Air Force Base, Mass.

1. INTRODUCTION

As discussed in Chapter 2, predictions of the infrared radiance are made principally on the basis of theoretical models that utilize observations of the atmospheric temperatures and species concentrations. Extensive measurements of these properties of atmosphere have been carried out over the past ten years using ground-based, rocket and satellite borne instruments. From these measurements a number of models have been developed to describe the behavior of the smooth atmospheric profiles that result from variations in the solar heating, magnetic activity, and motion of the earth.

In this chapter these models and measurements that support these models are reviewed briefly. Special emphasis is given to the Jacchia 77 (J77) model as this model has been selected as the basis for updating the high altitude infrared model to include the effects of atmospheric variability. This review will enable us to draw some inferences concerning the variability of the atmospheric infrared radiance that can result from the variations in species concentrations and

temperature. In Chapter 4 initial efforts to include some of the variations represented by these models in the calculation of the infrared radiance are presented.

2. ATMOSPHERIC MODELS

2.1 CIRA 72

In CIRA 72 (COSPAR, 1972[1]) the latest internationally adopted model, a mean COSPAR International Reference Atmosphere compiled by K.S. Champion and R.A. Schweinfurth for the altitude range 25 to 500 km is presented. This atmosphere represents average diurnal, seasonal, semiannual, and geomagnetic conditions appropriate to 30°N latitude and a 10.7 cm solar flux of 145 × 10^{-22} W m^{-2} Hz^{-1}. The resultant exospheric temperature is 1000 K. In addition, CIRA 72 presents tables of the atmospheric properties as functions of latitude, time of year for altitudes from 25 to 110 km due to G.V. Groves and tables of atmospheric profiles for altitudes from 110 to 1000 km with exospheric temperatures ranging from 500 to 2200 K, derived from the work of L. Jacchia.[2] Experimental data that support these models are also discussed, as well as the variations to be expected in these models.

2.2 USSA 76

The U.S. Standard Atmosphere 1976, (USSA 76) (COESA, 1976[3]) presents a single consistent model of globally averaged values of the atmospheric parameters for altitudes up to 1000 km. This model is assumed to be representative of moderate solar activity. The presentation of this model included a review of some features of the variation of atmospheric properties. Seasonal and latitudinal variations in the mean monthly temperature and density below 90 km are compared with average values of USSA 76 in Figures 1 and 2 and are in general agreement with similar results presented in CIRA 72. Figure 2 shows that variations of as much as 50 percent in density can occur at altitudes at which significant infrared radiation is produced. Such variations in temperature and density can lead to appreciable variations in the infrared radiance. The variation in species concentrations which result from variations in the temperature-height profiles at

---

1. COSPAR (1972) Committee on Space Research, CIRA 72, Cospar International Reference Atmosphere. Akademie-Verlag, Berlin.
2. Jacchia, L.G. (1977) Thermospheric Temperature, Density and Composition: New Models, SAO Special Report No. 375.
3. COESA (1976) Committee on Extension to the Standard Atmosphere, U.S. Standard Atmosphere Supplements, 1966, U.S. Government Printing Office, Washington, D.C.

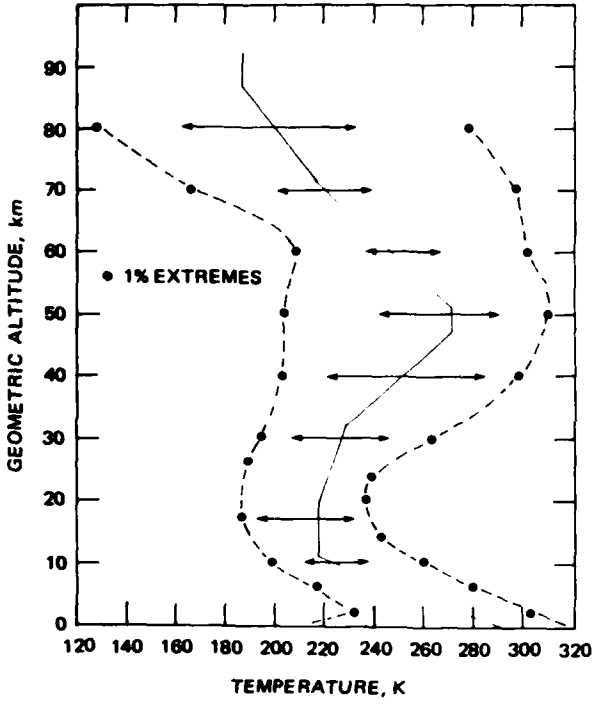

Figure 1. Range of Systematic Variability of Temperature Around the USSA 76 (COESA, 1976[3])

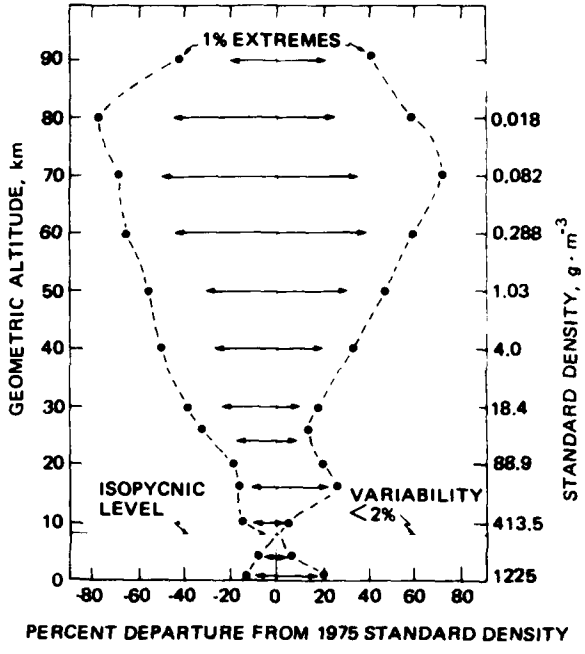

Figure 2. Range of Systematic Variability of Density Around the USSA 76 (COESA, 1976[3])

altitudes above 100 km for various degrees of solar and geomagnetic activity are also discussed in USSA 76.

2.3 Air Force Reference Atmospheres

Recently Cole and Kantor (1978)[4] published reference atmospheres that provide seasonal, latitudinal, and day-to-day variability of the thermodynamic properties of the atmosphere up to an altitude of 90 km. These models expand upon and update information contained in the USSA 76 (COESA, 1976[3]). Cole and Kantor[4] present sets of mean monthly reference atmospheres describing seasonal changes in the vertical distributions of temperature, density, and pressure for 15° intervals of latitude between the equator and pole. In addition, they present estimates of the day-to-day variations around the monthly median values of temperature and density. Figure 3 displays the latitudinal variations in average monthly temperature for the months of January and July. From these temperature profiles density profiles can be constructed using the barometric equation. The results of this calculation show density variations similar to those shown in Figure 2.

In arctic and subarctic regions, sudden warmings and coolings of the winter stratosphere and mesosphere produce large changes in the vertical and horizontal structure of the atmosphere, both in the magnitude and in the altitude region of the temperature and density fluctuations. The day-to-day variations in temperature are in some cases as great or greater than the seasonal or latitudinal changes. Although warmings and coolings occur throughout the artic and subartic regions, the largest changes generally occur between latitudes 60° and 75°.

2.4 MSIS

The MSIS model (Hedin et al, 1977a,[5] 1977b[6]) is a global thermospheric model that has been constructed from measurements of the density of N_2 with mass spectrometers on five satellites (AE-B, OGO 6, San Marco 3, Aeros A, and AE-C) and from neutral temperatures inferred from incoherent radar backscatter measurements at four ground stations (Arecibo, Jicamarca, Millstone Hill, and

---

4. Cole, A.E. and Kantor, A.J. (1978) Air Force Reference Atmospheres, AFGL-TR-78-0051, AD 058 505.

5. Hedin, A.E., Salah, J.E., Evans, J.V., Reber, C.A., Newton, G.P., Spencer, N.W., Kayser, D.C., Alcayde, D., Bauer, P., Cogger, L., and McClure, J.P. (1977a) A global thermospheric model based on mass spectrometer and incoherent scatter data, MSIS 1, N_2 density and temperature, J. Geophys. Res. 82:2139-2147.

6. Hedin, A.E., Reber, C.A., Newton, G.P., Spencer, N.W., Brinton, H.C., and Mayr, H.G. (1977b) A global thermospheric model based on mass spectrometer and incoherent scatter data, MSIS 2, Composition, J. Geophys. Res. 82:2148-2156.

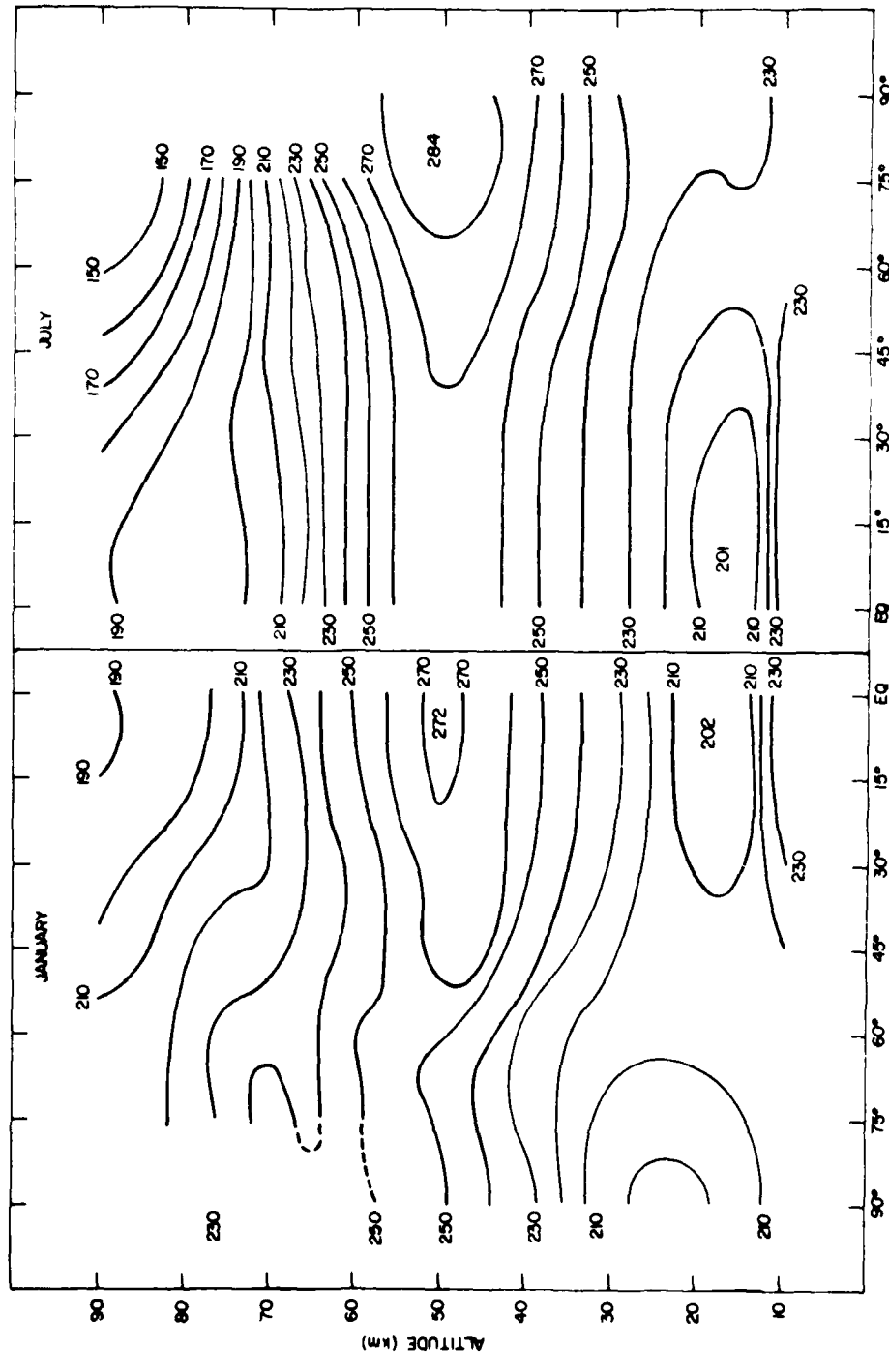

Figure 3. Latitudinal Temperature-height Cross Sections of Monthly Temperatures for January and July (Cole and Kantor, 1978[4])

St. Santin). The satellite and ground-based incoherent scatter measurements provide unique and complementary information on the structure of the thermosphere. In addition, the MSIS model combines measurements of the densities of O, He, and Ar from neutral-gas mass spectrometers on four satellites and inferred O_2 and H densities from an ion mass spectrometer on the AE-C satellite with the neutral temperature and N_2 density models to produce a global model of thermospheric composition in terms of inferred variations at 120 km. The overall data set of these measurements covers the time period from the end of 1965 to mid-1975. In MSIS the exospheric temperature and other quantities are represented by least squares fits to the data in spherical harmonic expansions. In 1979 the MSIS model was extended to include longitudinal and universal time (UT) variations in thermospheric neutral temperature and composition (Hedin et al, 1979[7]). Terms that depend only on longitude indicate a temperature enhancement at 120 km of about 30°K at a latitude of approximately 70° along the longitude of the magnetic poles. As with the variations with magnetic activity, the extrapolated 120 km variations are generally in phase with temperature variations for N_2, Ar, and O_2 and out-of-phase for He, O, and H. The combined longitude and UT variations reflect the influence of the earth's magnetic field and suggest that the primary variations may be simply represented in magnetic coordinates.

The MSIS model is most representative of magnetically quiet conditions with the best data coverage between altitudes 200 and 600 km and with solar $F_{10.7}$ indices between 75 and 180. The species concentrations should be reasonably valid above 150 km, but below 150 km they are essentially extrapolations from higher altitudes. Temperatures below 200 km may not adequately represent diurnal and semidiurnal variations. The limitations on altitudes make the application of the MSIS model to the calculation of limb viewing infrared calculations very difficult. In addition, the use of spherical harmonic construction of this model make it difficult to join to the lower altitude atmospheric models.

2.5 Jacchia 77 (J77)

The Smithsonian Astronomical Observatory models (Jacchia, 1977[2]) that describe the thermospheric temperature, density, and composition consist of essentially two parts: 1) the basic static models, that give temperature and density profiles of the atmospheric constituents for any specified exospheric temperature and 2) a set of formulae for correcting the exospheric temperature based on various types of thermospheric variation.

---

7. Hedin, A.E., Reber, C.A., Spencer, N.W., Brinton, H.C. and Kayser, D.C. (1979) Global model of longitude/UT variations in thermospheric composition and temperature based on mass spectrometer data, J. Geophys. Res. 84:1-9.

The Jacchia models are based primarily on a very large number of satellite drag measurements and on composition measurements from several satellites, OGO-6, ESRO 4, and S3-1. For the basic static models, tables of temperature, species concentrations, pressure and mass density are given for altitudes from 90 to 2500 km and for exospheric temperatures from 500 to 2600 K. The temperature profiles start from a constant value of 188 K at an altitude of 90 km, rise to an inflection point of 125 km, and become asymptotic to an "exospheric" temperature at approximately 500 km. Examples of the resultant temperature profiles are shown in Figure 4. The mass density is assumed to have a constant value of 3.43×10^{-6} kg/m^3 at the altitude of 90 km. The atmosphere is assumed to be composed of N_2, O_2, O, Ar, He, and H with constant mixing ratios up to 100 km and with abundances determined by diffusive processes above this height. Number density profiles of the major atmospheric species for two exosphere temperatures are illustrated in Figure 5. The assumption of fixed boundary conditions at 90 km can lead to discontinuities in the density and temperature profiles if the Jacchia model is joined to atmospheric models that describe the mesosphere. Indications of the possible density variability and temperature variability at 90 km are shown in Figures 1, 2, and 3.

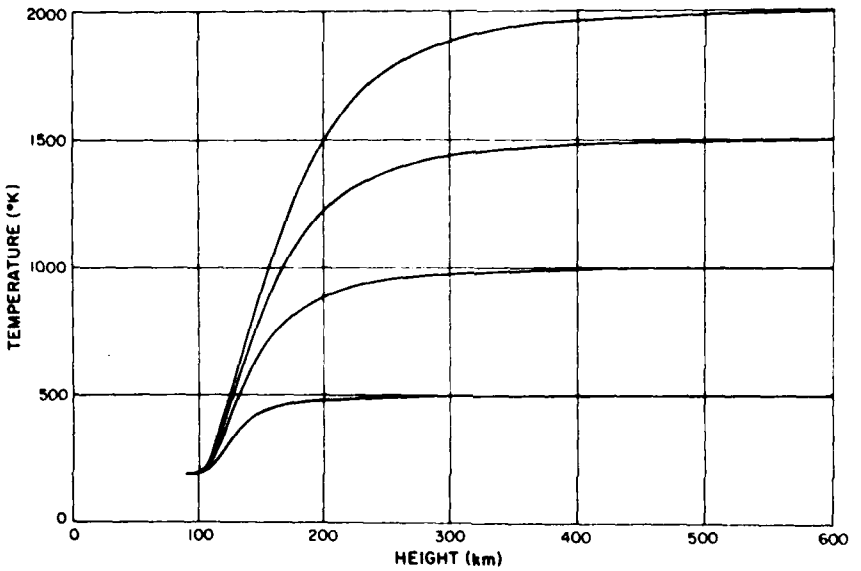

Figure 4. Four Temperature Profiles from the J77 Model (Jacchia, 1977[2])

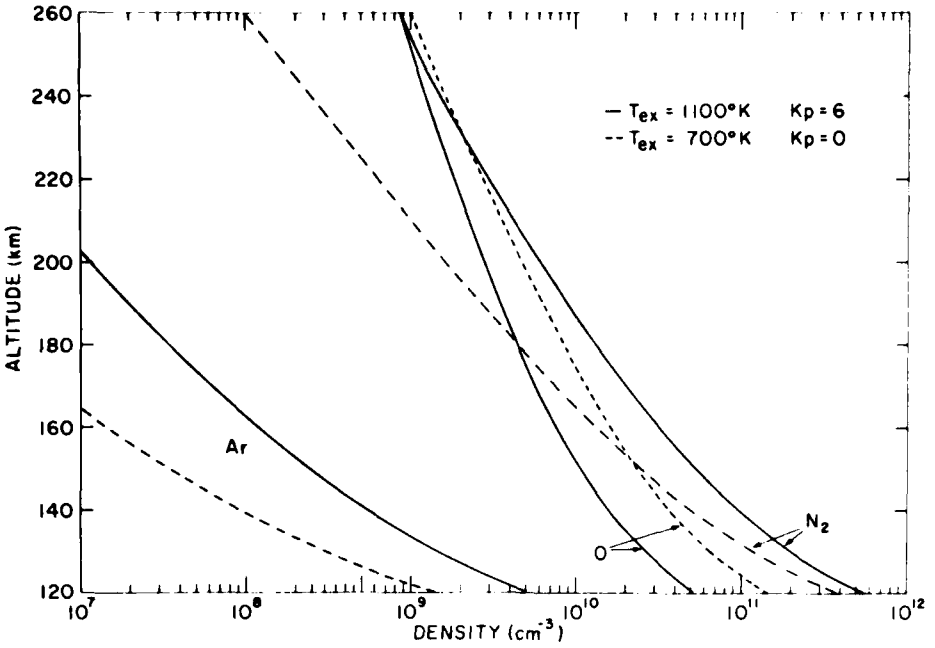

Figure 5. Variations of Atmospheric Species Concentrations at 78° Latitude as Predicted by J77 Model Under Two Conditions of Geomagnetic Activity and Exospheric Temperature

The types of variation that the J77 models attempt to represent can be classified as follows:

1. Variation with solar cycle
2. Variation with changes in activity on the disk of the sun
3. The daily or diurnal variation
4. Variations with geomagnetic activity
5. Seasonal-latitudinal variations
6. The semiannual variation

All these variations are based on parameters that can be predicted with varying degrees of accuracy or can be obtained from observational data. Such static models should be quite adequate to describe the mean conditions when the characteristic time of the variation is much longer than the time scale of conduction, convection, and diffusion processes. The following paragraphs describe how the above variations are incorporated by Jacchia.

The magnitude of the variation of the exospheric temperature is represented as a function of both the instantaneous value of the 10.7-cm solar flux F and the flux averaged over a few solar rotations $\bar{F}$. The variation of exospheric

temperature is applied with a time lag that varies from 0.9 days at noon local solar time (LST) to 1.6 days at midnight LST.

The diurnal variation of the exospheric temperature is represented as the sum of two terms, one representing a seasonal-latitudinal variation that is independent of local time and another that is a function of local time. The seasonal-latitudinal (or annual) variation has a maximum value of 15 percent at the poles and is proportional to the declination of the sun and to the sine of the latitude. In Figure 6 the resulting variations of exospheric temperature at the equinoxes and the June solstice are shown for quiet magnetic conditions ($K_p = 0$). This global variation of exospheric temperature, in conjunction with the resulting variation in species concentrations, can produce a variation in the global infrared emission. Examples of such variations are shown in Chapter 4.

The variation with geomagnetic activity is represented as a temperature increase that is a function of the geomagnetic latitude and the K_p index. The accompanying variation in species concentrations is comprised of three separate components: a thermal component due to the change in scale height induced by the change in temperature, a component due to the change in the altitude of the homopause (the interface between the regimes of mixing and diffusion), and a component due to the "equatorial wave" that results from a density enhancement resulting from convection toward the equator. An example of the resulting change in exospheric temperature is shown in Figure 7, where it is seen that the temperature at the higher latitudes can be significantly changed by magnetic activity. The effective change in the altitude of the homopause included in the model is shown in Figure 8 as a function of K_p for various geomagnetic latitudes. The density variations of four atmospheric constituents as a function of the invariant magnetic latitude for a $K_p = 5$ are shown in Figure 9. The effect of the geomagnetic correction to the J77 model is also shown in the profiles presented in Figure 5.

A recent modification of the J77 model (Philbrick and Gardner, 1980[8]) predicts the nighttime altitude profile of CO_2 as a function of latitude and geomagnetic activity. In Figure 10 the variation in this important infrared contributor is shown for low and high latitudes and for a range of geomagnetic activity. These results suggest that particularly significant variations in the infrared radiation from CO_2 may occur with the variation in geomagnetic activity. Calculations of the radiation from CO_2 presented in Chapter 4 demonstrate this effect.

---

8. Philbrick, C.R. and Gardner, M.E. (1980) Private communication.

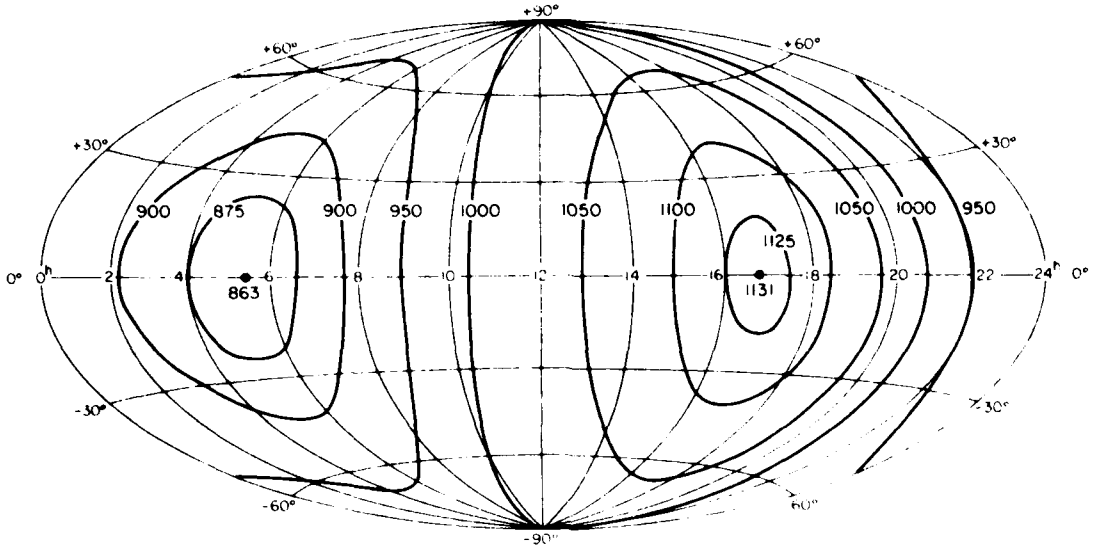

a) EQUINOXES

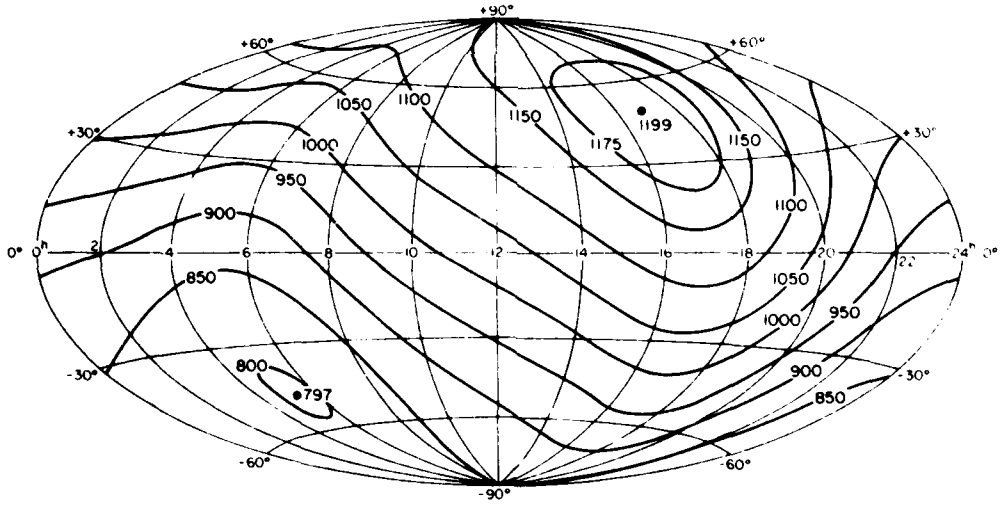

b) JUNE SOLSTICE

Figure 6. Global Distribution of the Exospheric Temperature for Quiet Geomagnetic Conditions ($K_p = 0$). The coordinates are local solar time and geographic latitude (Jacchia 1977[2])

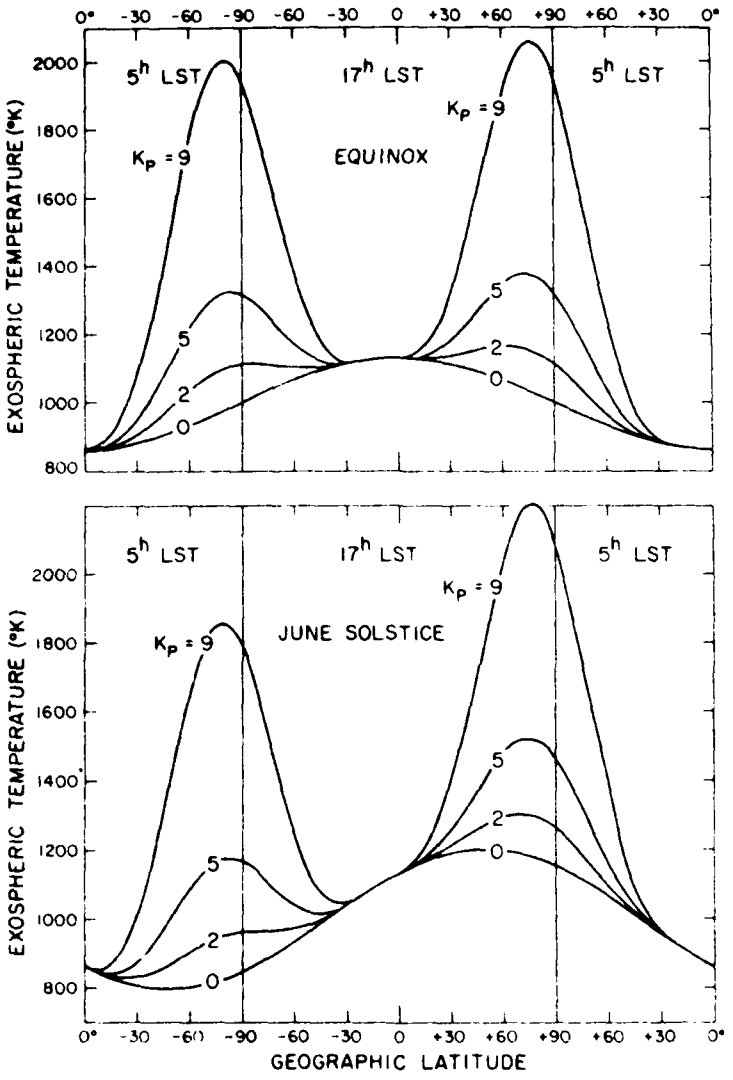

Figure 7. Exospheric Temperature Profiles Along the Complete (360°) Meridional Circle Along Which the Local Solar Time is 17^h in One Hemisphere and 5^h in the Other, for Various Levels of Geomagnetic Activity. Even a moderate level of activity ($K_p \approx 2$) has the effect of shifting the temperature maximum from the equator to the poles at the time of equinoxes (Jacchia, 1977[5])

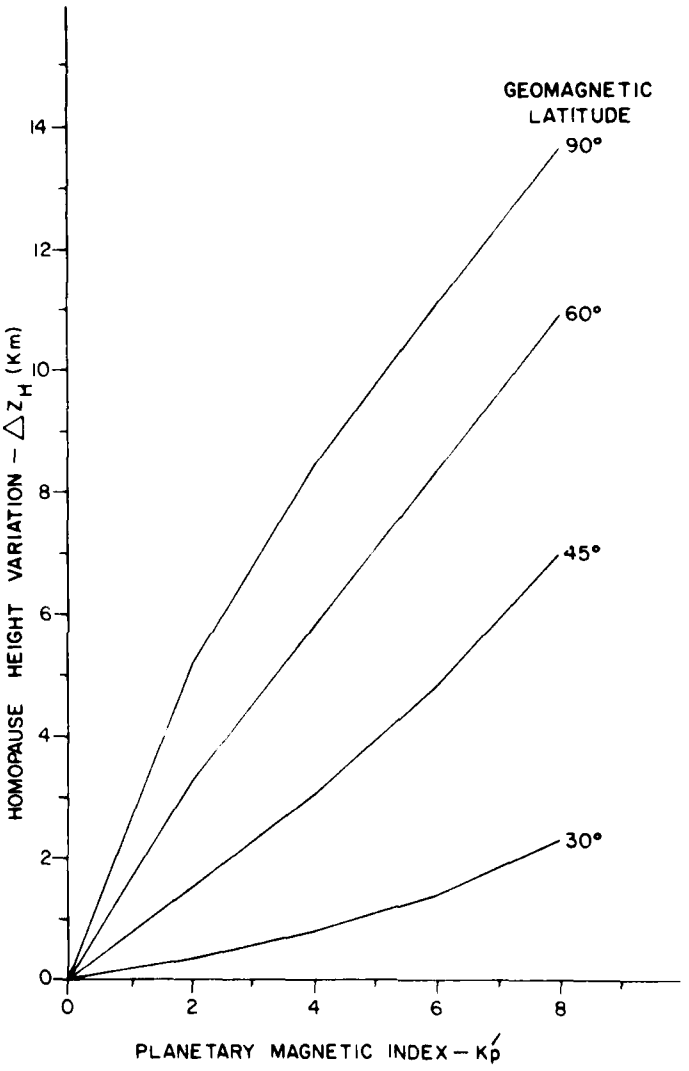

Figure 8. Hemopause Height Variation vs K_p' for Several Geometric Latitudes (J77 Model)

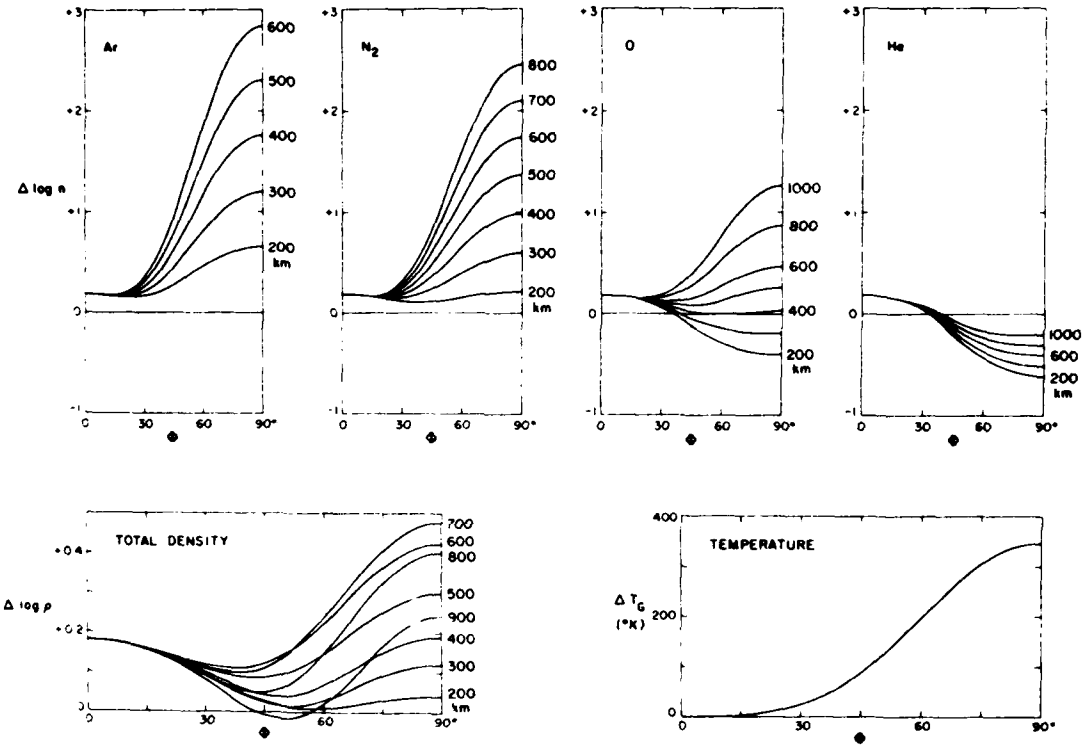

Figure 9. The Density Variation of Four Atmospheric Constituents as a Function of the Invariant Latitude ϕ, for Various Heights When the Geomagnetic Index K_p = 5. The curves were computed using a "quiet" (K_p = 0) exospheric temperature of 900 K. The diagram in the lower left corner depicts the variation of the total density; that in the lower right corner gives the corresponding variation in the exospheric temperature (Jacchia, 1977[2])

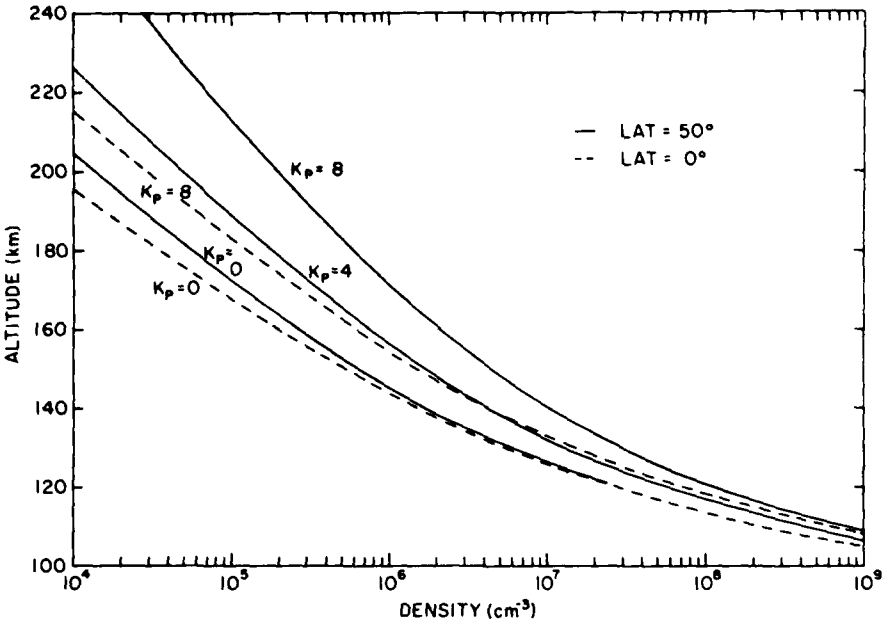

Figure 10. CO_2 Atmospheric Density Predictions Based on the Jacchia Model at Latitudes of 0° and 50° for Nighttime Conditions

3. ATMOSPHERIC MEASUREMENTS COMPARED WITH MODELS

Various measurements have been compared to the predictions of the above models. These comparisons show that the J77 and MSIS models are in general agreement. However, neither provides a completely satisfactory representation of the atmosphere. For example, in Figure 11 altitude profiles of N_2, Ar, O, and O_2 number densities measured during the Aladdin 74 program (Trinks et al, 1978[9]) are compared to the predictions of the J77 and MSIS models. The dip in the densities by a factor of 3 to 5 at 112.5 km is indicative of the variations in the lowest part of the thermosphere. Trinks et al[9] suggested that this variation could be the superposition of a semidiurnal tidal wave and a gravity wave. This proposition was supported by the temperature-height profile obtained from incoherent-scatter radar measurements.

Figures 12 and 13 show the comparison of model prediction and measurements at higher altitudes. Predictions of the N_2, O, and Ar density models using the J77 and MSIS are compared to measurements made with the S3-1 satellite

9. Trinks, H. and Fricke, K.H. (1978) Carbon dioxide concentrations in the lower thermosphere, J. Geophys. Res. 83:3883-3886.

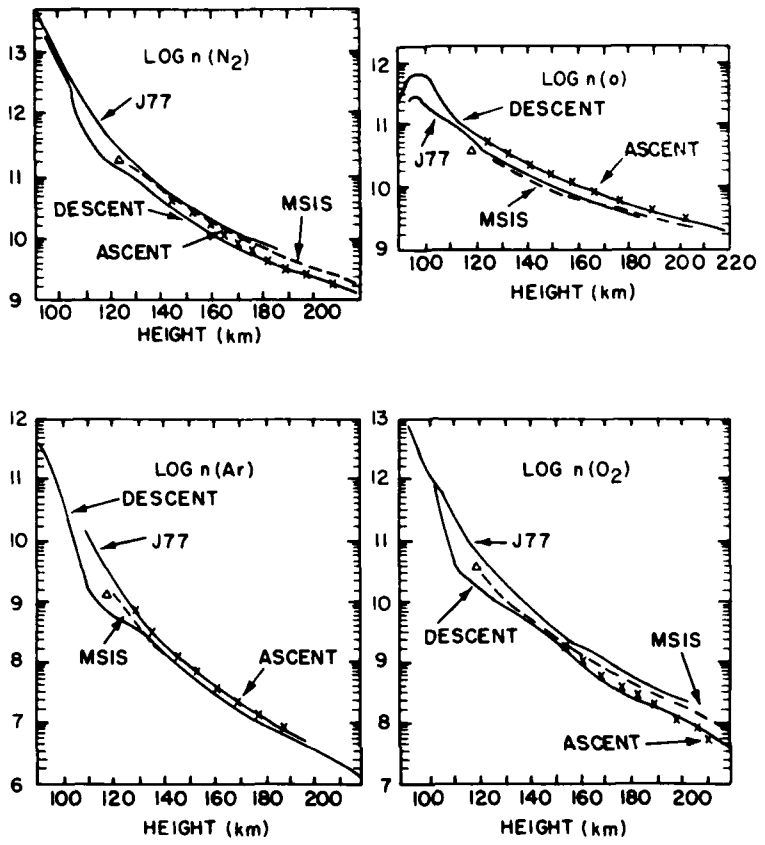

Figure 11. Density-height Profiles of N_2, Ar, O, and O_2. The dots and heavy solid curves represent the descent data; the ascent data are given by the dashed curves. The number densities are in units per cm^3 and on a logarithmic scale. Also shown are the predictions of the Jacchia 77 model (J77) and the MSIS model (Hedin, et al, 1977a,[5] 1977b[6]); the triangles denote rocket averages (Offerman, 1974[10]), (Trinks et al, 1978[9])

(Philbrick and Gardner 1980[8]) for both magnetically quiet and disturbed conditions. The differences between the models and the data show that, while general agreement exists, the observed small-scale variations of the densities are not modeled. It is also evident from these two typical cases that, during a period of higher geomagnetic activity, such as shown in Figure 13, significantly more structure is observed in the profiles.

---

10. Offerman, D. (1974) Composition variations in the lower thermosphere, J. Geophys. Res. 79:4281-4293.

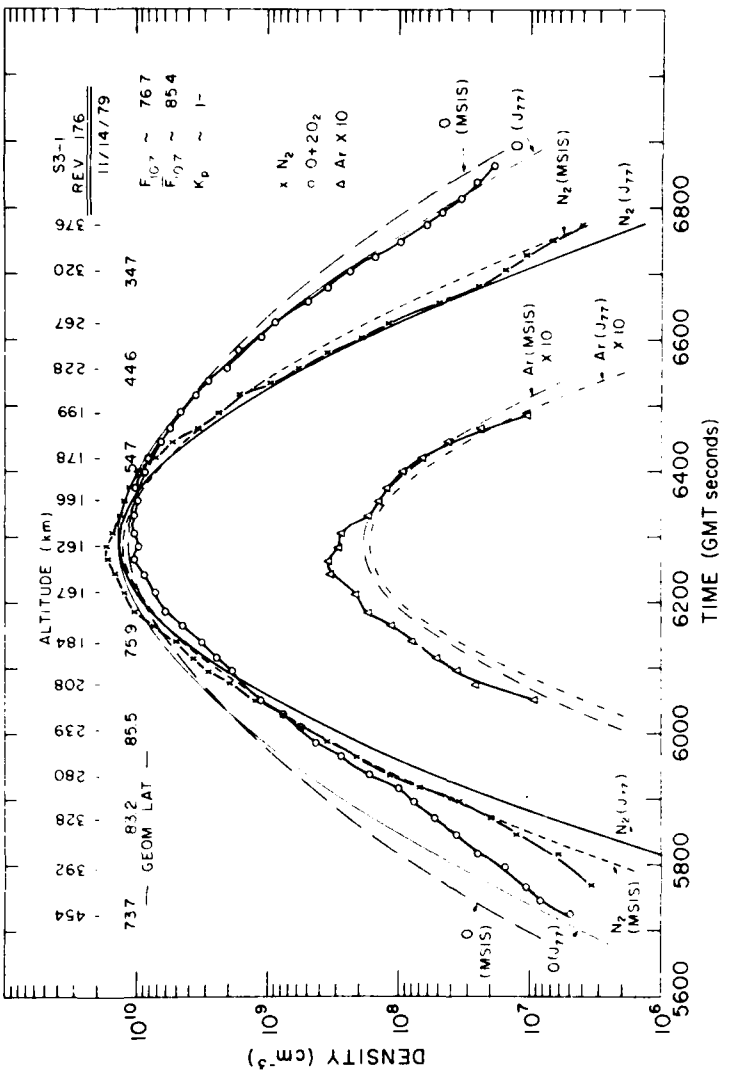

Figure 12. Comparison of Predictions of J77 and MSIS Models for N_2, O, and Ar With Measurement Made During S3-1 Satellite Flight Under Magnetically Quiet Conditions

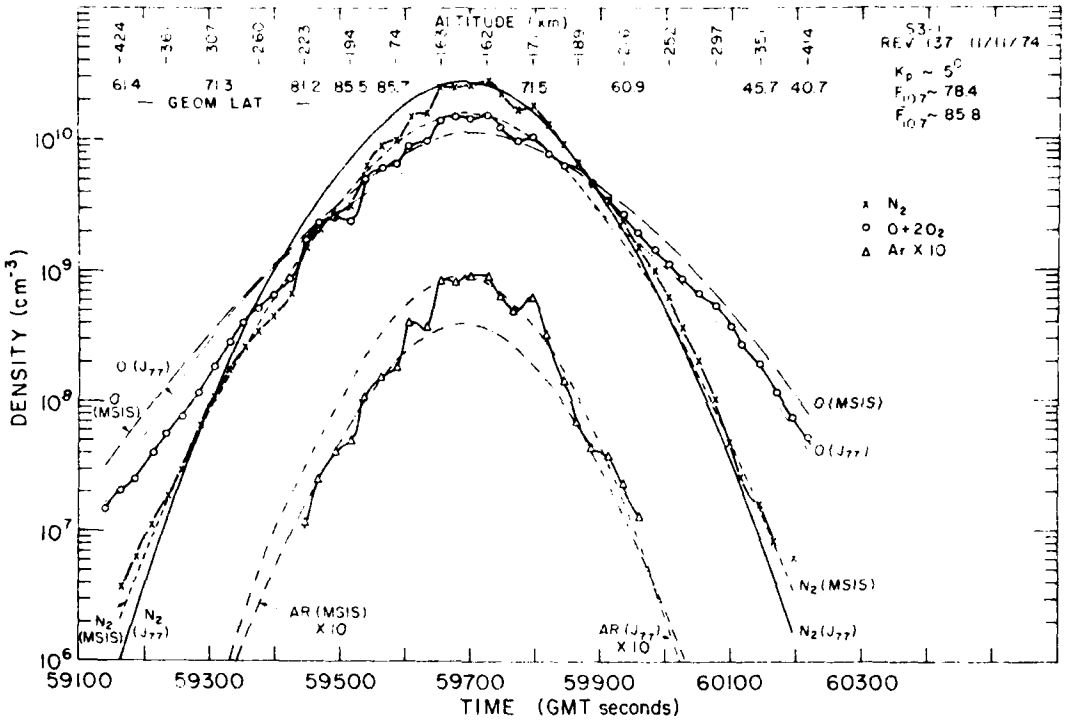

Figure 13. Comparison of Predictions of J77 and MSIS Models for N_2, O, and Ar With Measurements Made During S3-1 Satellite Flight Under Magnetically Disturbed Conditions

4. GEOMAGNETIC INDUCED VARIATIONS OF SPECIES CONCENTRATIONS

The influence of geomagnetic activity on the upper atmospheric species densities is even stronger than it is upon the total mass density. This effect is due to the difference in diffusion velocities of the various species and results in depletions of those species with mass lighter than the mean molecular weight (see, for example, the predictions of the Jacchia 77 model in Figures 5 and 10). Figure 13 shows that disturbed magnetic conditions ($K_p = 6^+$) can greatly increase N_2 density, Ar density, and the structure in the density profiles.

In Figure 14 the correlation of species concentrations with geomagnetic activity is studied further. It is seen that the Ar/N_2 ratio, as well as the total density, is strongly correlated with the level of geomagnetic activity. The Ar density is highly correlated with the level of geomagnetic activity whereas, the O density appears to have a weak negative correlation with K_p, about 30 percent change in this case. The large increase in Ar density with K_p is shown further in Figure 15, where measurements made by the S3-1 satellite are plotted versus geomagnetic latitude for two ranges of K_p, $0 \leq K_p \leq 2^+$ and $4 \leq K_p \leq 6^+$. The dependence on geomagnetic activity of CO_2 is expected to be similar to that of Ar due to the nearly equal atomic masses. Thus, the effect of increased geomagnetic activity upon atmospheric infrared radiance should be very important. The influence of photochemical processes on this connection is considered in the next section.

In Figure 16 estimates of the frequency of occurence of high magnetic activity and of the duration of such increases are shown. These estimates are from the work of Pazick (1976).[11] He presented tables of probabilities of geomagnetic activity. In particular, these results indicate that approximately one-sixth of the time K_p will exceed 4 and approximately one-half these disturbances will last longer than one day.

5. VARIATIONS IN CONCENTRATIONS OF THE MINOR ATMOSPHERIC SPECIES

Direct measurements of the minor atmospheric species have been carried out from rocketborne platforms. The results of these measurements make it possible to draw some conclusions concerning the overall variability of the minor species, but few conclusions can be drawn concerning the time dependence of these variations.

---

11. Pazick, P. M. (1976) Conditional Probabilities of the Geomagnetic Index A_p, AFGRL-TR-76-0034, AD A023 675.

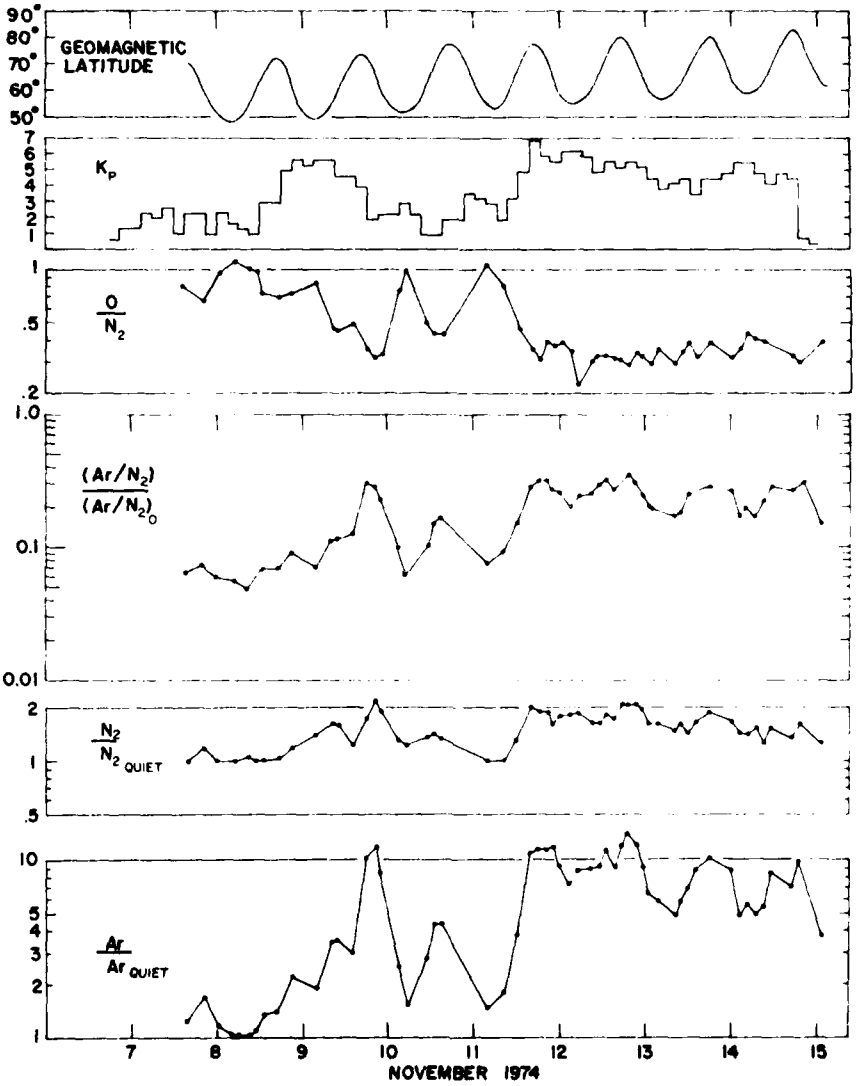

Figure 14. Correlation of Species Concentration at an Altitude of 160 km With Geomagnetic Activity During a Magnetic Storm from 7 November to 15 November 1974

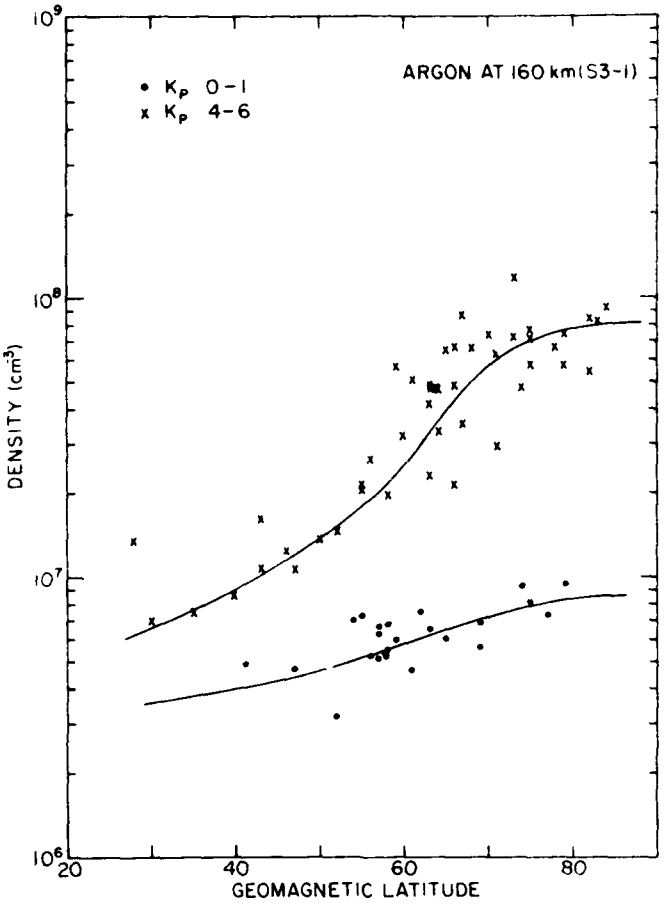

Figure 15. Ar Density at an Altitude of 160 km as a Function of Geomagnetic Latitude for Quiet and Disturbed Magnetic Conditions

Measurements of the density of CO_2 by mass spectrometer (Philbrick et al, 1973[12]) have shown that CO_2 is mixed in its ground level ratio between 85 and 100 km. Measurements of the CO_2 density above the turbopause were performed at night in 1973 by Offermann and Grossman (1973)[13] and during the day in 1974

12. Philbrick, C.R., Faucher, G.A. and Trzcinski, E. (1973) Rocket measurements of mesospheric and lower thermospheric composition, Space Research XIII:255-260.

13. Offerman, D. and Grossman, K.U. (1973) Thermospheric density and composition as determined by a mass spectrometer with cryo ion source, J. Geophys. Res. 78:8296-8304.

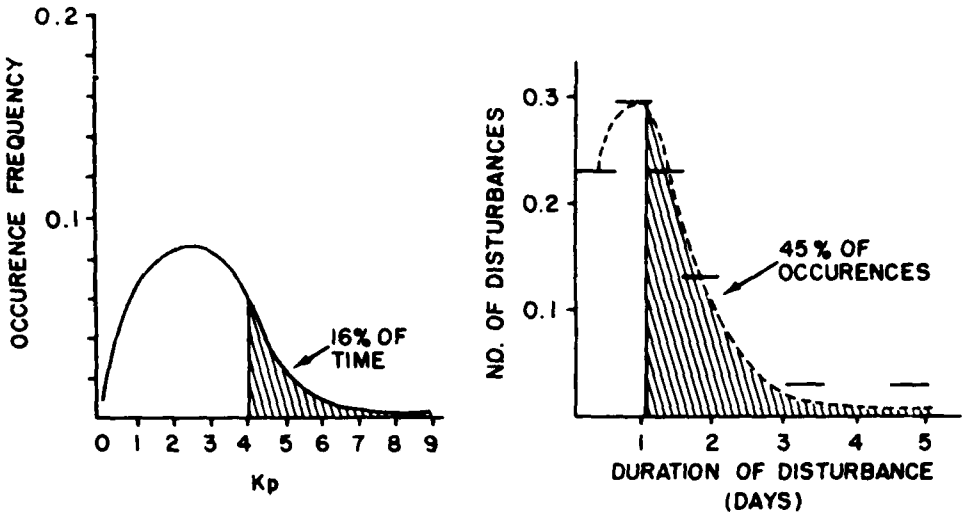

Figure 16. Summary of Disturbed Atmosphere Frequency or Occurrence (geomagnetic disturbances only) for Solar Maximum Years

by Trinks and Fricke (1978).[9] In Figure 17, these results are plotted as ratios to the Ar density. At night it is found that the CO_2/Ar ratio follows the expected diffusive equilibrium profile, while during the day the ratio decreases from the diffusive profile by a factor of about 3 at 140 km. This result is in agreement with the loss of CO_2 by solar dissociation and reaction with O^+ ions. The fact that the CO_2 density responds in a similar way to the Ar density makes it possible to infer the behavior of fluctuations in the CO_2 density from measurements of the fluctuations in the Ar density, especially at higher altitudes.

A midlatitude model of the ozone density constructed by A.J. Kruger and R.A. Minzner[14] was presented in USSA 76. Figure 18 (a and b) shows the resultant O_3 concentration, as well as the O_3 mass mixing ratio. Expected variations of the density and mixing ratio of O_3 are also shown in these figures. From Figure 18 (a) it is seen that at high altitude the O_3 concentration varies by as much as a factor of three. During the Aladdin program in 1974, measurements of the O_3 density (Weeks et al, 1978[15]) were made at altitudes from 19 to 108 km using four different techniques. Results of these measurements are shown in Figure 19 (a, b, and c) for three separate altitude regions. These results are in basic

14. Kruger, A.J. and Minzner, R.A. (1976) A midlatitude ozone model for the 1976 U.S. standard atmosphere, J. Geophys. Res. 81:4477-4481.

15. Weeks. L.H., Good, R.E., Randhawa, J.S. and Trinks, H. (1978) Ozone measurements in the stratosphere, mesosphere, and lower thermosphere during Aladdin 74, J. Geophys. Res. 83:978-982.

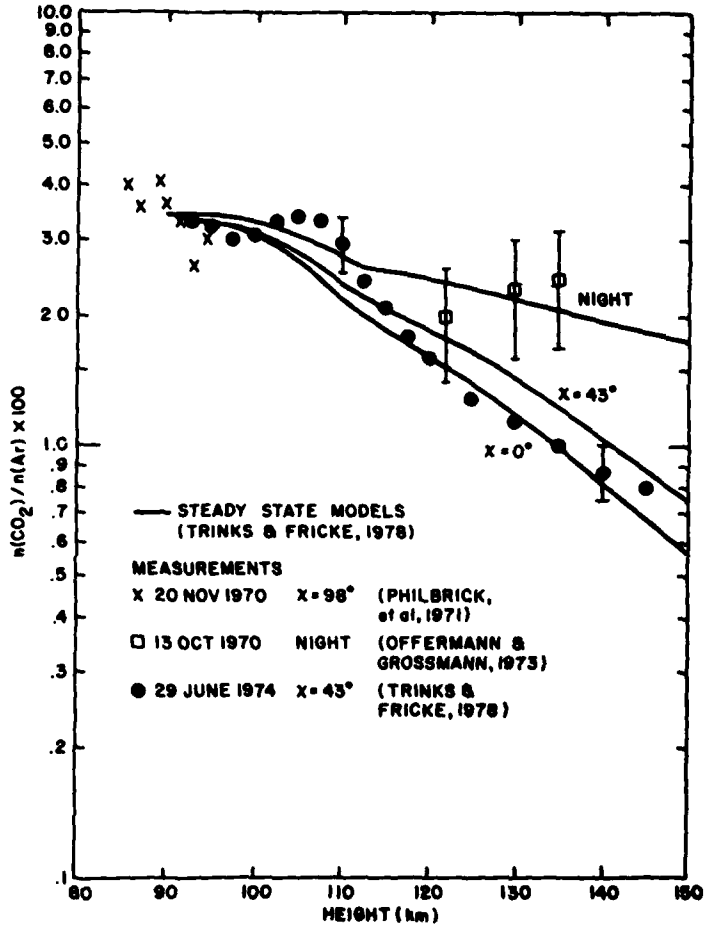

Figure 17. Calculated and Measured $n(CO_2/n(Ar)$ Ratio for Two Background Atmospheres and Three Solar Zenith Angles. Data are from Trinks and Fricke (1978)[9] (solid circles), Offermann and Grossmann (1973)[13] (squares) and from Philbrick et al, (1971).[16] [Source – Trinks and Fricke (1978)[9]]

agreement with the model presented in Figure 18 (a and b). In Figures 19 (a, b, and c) these results are also compared to other models of the O_3 density. These measurements reveal a structured density profile at altitudes above 75 km, particularly for measurements made with the airglow photometer. These variations

16. Philbrick, C.R., Faucher, G.A., and Wlodyka, R.A. (1971) Neutral Composition Measurements of the Mesosphere and Lower Thermosphere, AFCRL-71-0602, AD 739169.

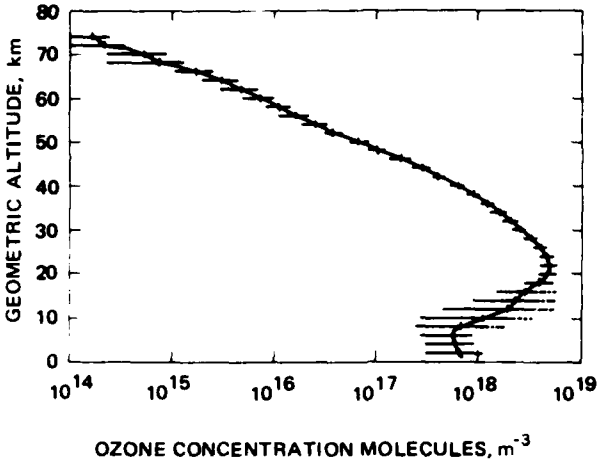

(a) Density as a Function of Height

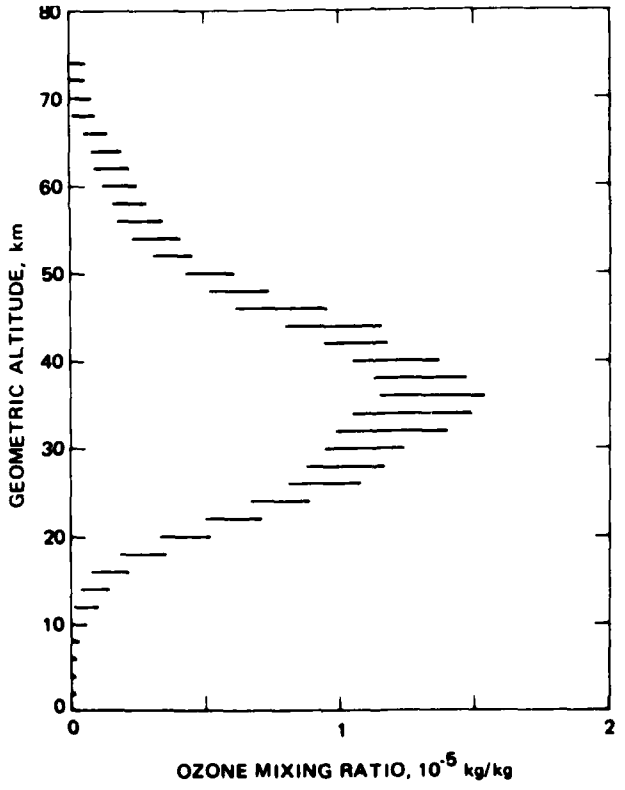

(b) Mixing Ratio as a Function of Height

Figure 18. Midlatitude Ozone Model (COESA, 1976[3])

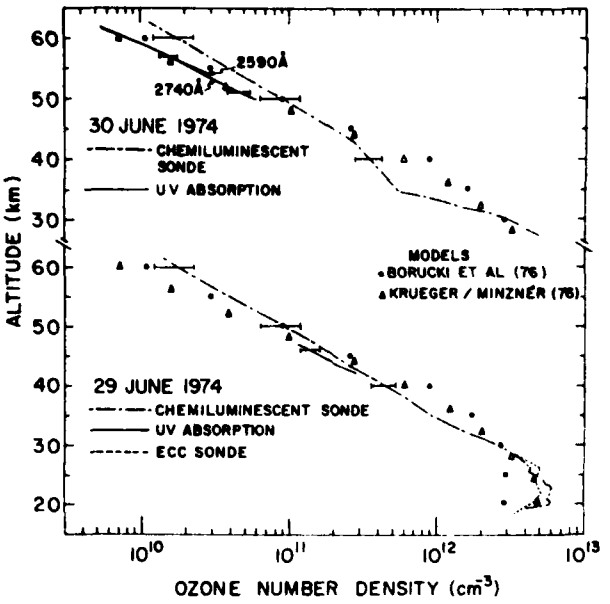

Figure 19a. Chemiluminescent Sonde O_3 Data Compared With UV Results, ECC Sonde, and Models (Weeks et al, 1978[15])

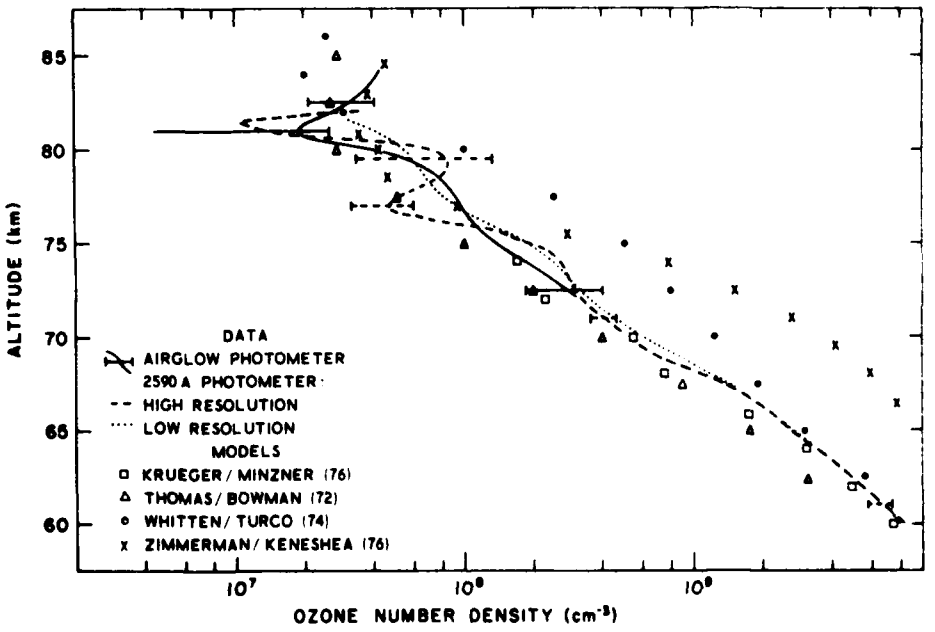

Figure 19b. Comparison of UV and Airglow Techniques for O_3 Determination (Weeks et al, 1978[15])

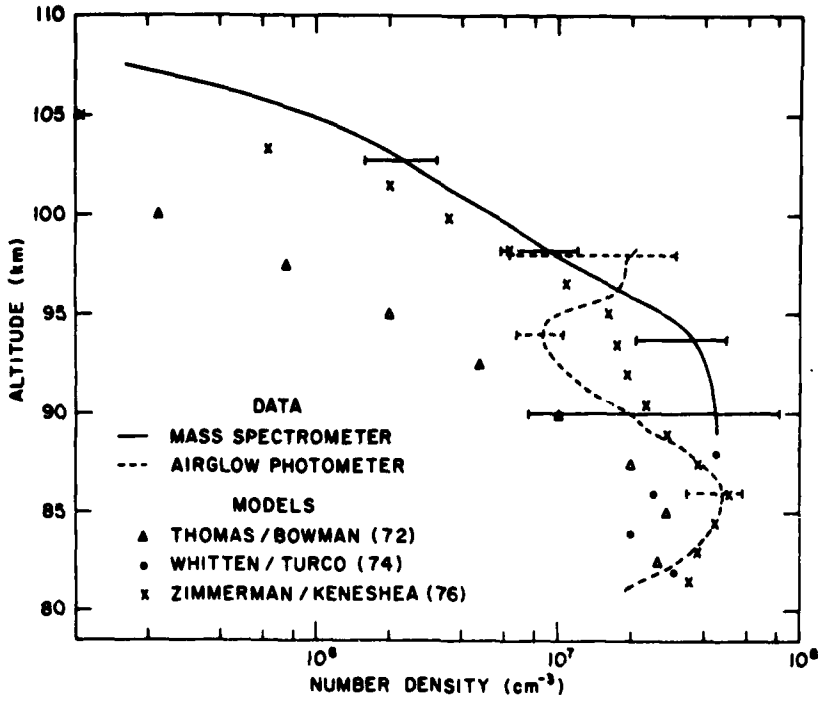

Figure 19c. Comparison of Airglow and Mass Spectrometer Results for O_3 Determination With Some Typical Models (Weeks et al, 1978[15])

appear to have similar scale sizes and amplitudes as those found in the atomic oxygen profiles that are discussed in Chapter 5.

Using resonantly scattered light from thermospheric NO, measurements made aboard the Atmosphere Explorer C satellite have been used to study the dependence of the NO density on latitude, longitude, and magnetic activity. These results have been analyzed by T.E. Cravens and A.I. Stewart (1978)[17] to determine the NO density at an altitude of 105 km. They find that near the equator the density at the peak of the NO concentration is about 2×10^7 cm^{-3} and varies little with longitude or magnetic activity, except during major geomagnetic storms. As shown in Figure 20, the peak NO densities are typically two to three times larger and more variable at higher latitudes. Cravens and Stewart[17] found an increase in the NO density of as much as 30 percent at a latitude of 40°N and S. In addition to these effects, they found that the NO density at these latitudes doubles during times of high geomagnetic activity at ($K \simeq 6$). They also studied the

17. Cravens, T.E. and Stewart, A.I. (1978) Global morphology of nitric oxide in the lower E region, J. Geophys. Res. 83:2446-2452.

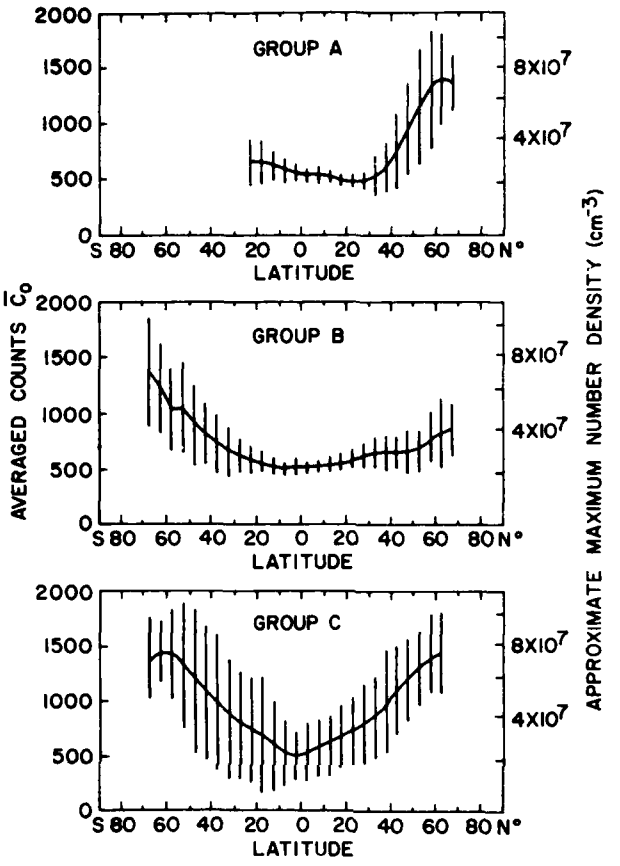

Figure 20. NO Signal from 105 km Zonally Averaged for Each of the Three Orbit Groups as Functions of Latitude. The bars are standard deviations

diurnal and seasonal effects at low latitudes and found that NO increases at the equator by a factor of 2 between sunrise and early afternoon with a small decline near sunset and that the density of NO is higher during the summer than during the winter.

References

1. COSPAR (1972) Committee on Space Research, CIRA 72, Cospar International Reference Atmosphere. Akademie-Verlag, Berlin.

2. Jacchia, L.G. (1977) Thermospheric Temperature, Density and Composition: New Models, SAO Special Report No. 375.

3. COESA (1976) Committee on Extension to the Standard Atmosphere, U.S. Standard Atmosphere Supplements, 1966, U.S. Government Printing Office, Washington, D.C.

4. Cole, A.E. and Kantor, A.J. (1978) Air Force Reference Atmospheres, AFGL-TR-78-0051, AD 058 505.

5. Hedin, A.E., Salah, J.E., Evans, J.V., Reber, C.A., Newton, G.P., Spencer, N.W., Kayser, D.C., Alcayde, D., Bauer, P., Cogger, L. and McClure, J.P. (1977a) A global thermospheric model based on mass spectrometer and incoherent scatter data, MSIS1, N_2 density and temperature, J. Geophys. Res. 82:2139-2147.

6. Hedin, A.E., Reber, C.A., Newton, G.P., Spencer, N.W., Brinton, H.C. and Mayr, H.G. (1977b) A global thermospheric model based on mass spectrometer and incoherent scatter data, MSIS2, Composition, J. Geophys. Res. 82:2148-2156.

7. Hedin, A.E., Reber, C.A., Spencer, N.W., Brinton, H.C. and Kayser, D.C. (1979) Global model of longitude/UT variations in thermospheric composition and temperature based on mass spectrometer data, J. Geophys. Res. 84:1-9.

8. Philbrick, C.R. and Gardner, M.E. (1980) Private communication.

9. Trinks, H. and Fricke, K.H. (1978) Carbon dioxide concentrations in the lower thermosphere, J. Geophys. Res. 83:3883-3886.

10. Offerman, D. (1974) Composition variations in the lower thermosphere, J. Geophys. Res. 79:4281-4293.

11. Pazick, P.M. (1976) Conditional Probabilities of the Geomagnetic Index A_p, AFGRL-TR-76-0034, AD A023 675.

12. Philbrick, C.R., Faucher, G.A. and Trzcinski, E. (1973) Rocket measurements of mesospheric and lower thermospheric composition, Space Research XIII:255-260.

13. Offerman, D. and Grossman, K.U. (1973) Thermospheric density and composition as determined by a mass spectrometer with cryo ion source, J. Geophys. Res. 78:8296-8304.

14. Kruger, A.J. and Minzner, R.A. (1976) A midlatitude ozone model for the 1976 U.S. standard atmosphere, J. Geophys. Res. 81:4477-4481.

15. Weeks, L.H., Good, R.E., Randhawa, J.S. and Trinks, H. (1978) Ozone measurements in the stratosphere, mesosphere, and lower thermosphere during Aladdin 74, J. Geophys. Res. 83:978-982.

16. Philbrick, C.R., Faucher, G.A., and Wlodyka, R.A. (1971) Neutral Composition Measurements of the Mesosphere and Lower Thermosphere, AFCRL-71-0602, AD 739169.

17. Cravens, T.E. and Stewart, A.I. (1978) Global morphology of nitric oxide in the lower E region, J. Geophys. Res. 83:2446-2452.